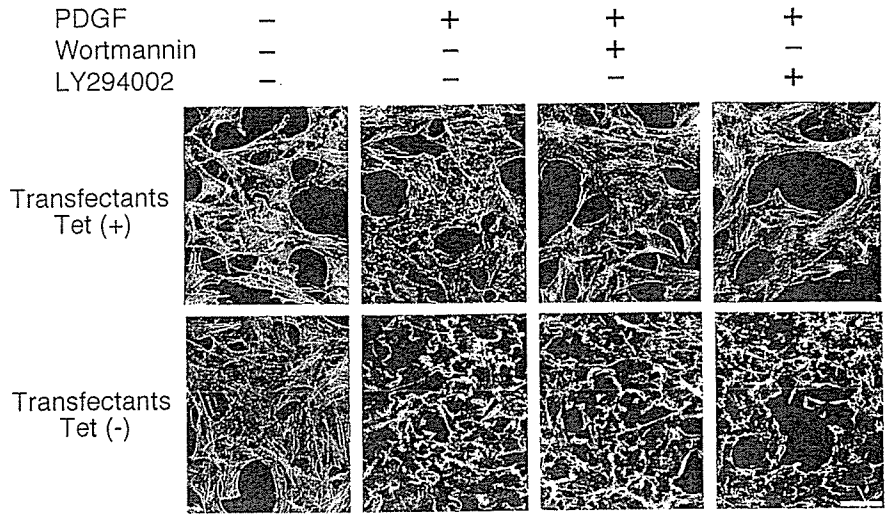

FIG. 3. **Effects of PI3K inhibitors on membrane ruffling of Iba1-expressing Swiss 3T3 cells.** Serum-starved Swiss 3T3 transfectants cultured in the presence or absence of tetracycline were pretreated with or without 100 nM wortmannin or 50 μM LY294002 for 30 min and then stimulated with 3 ng/ml PDGF for 10 min. The cells were fixed and stained with Texas Red-phalloidin. *Scale bar*, 50 μm.

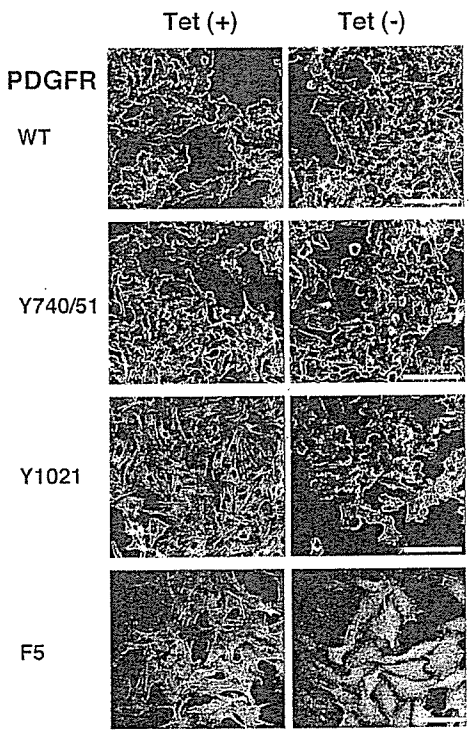

FIG. 4. **PLC-γ-dependent membrane ruffling of PDGF-stimulated PAE cells expressing Iba1 and WT or a series of PDGFR mutants.** WT-, Y740/51-, Tyr-1021-, and F5-PDGFR-expressing PAE Iba1 transfectants cultured in the presence or absence of tetracycline were each stimulated with 50 ng/ml PDGF for 5 min, then fixed and stained with Texas-Red phalloidin. *Scale bar*, 50 μm.

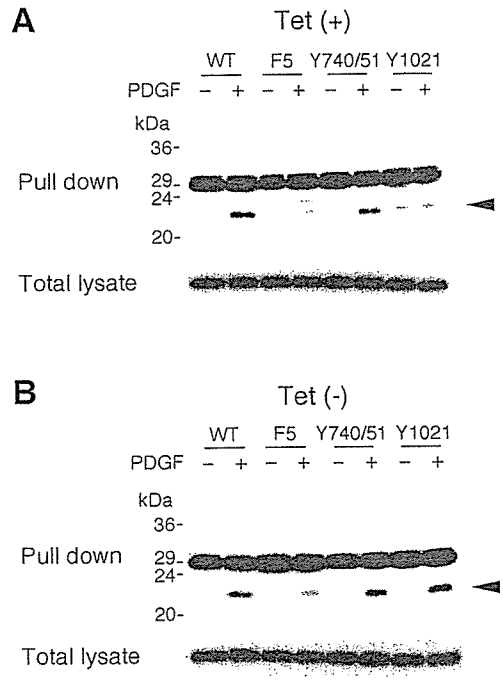

FIG. 5. **PLC-γ-dependent Rac activation in Iba1-expressing PAE cells.** PAE Iba1 transfectants expressing WT or PDGFR mutants cultured in the presence (*A*) or absence (*B*) of tetracycline were stimulated with or without 50 ng/ml PDGF for 2 min. After stimulation, the cells were lysed and GTP-bound active Rac was precipitated with GST-PAK-bound glutathione-Sepharose-4B beads. GTP-bound Rac (*upper panels*) and total Rac in the cell lysates (*lower panels*) were identified by Western blotting with an anti-Rac antibody. *Arrowheads* indicate positions of Rac. Highly intense bands migrating around 29 kDa correspond to GST-PAK protein.

Requirement of Iba1 in PLC-γ-dependent Rac Activation—Iba1 was recently demonstrated to function together with Rac in the membrane ruffling of microglia, and Rac was shown to be activated during their membrane ruffling (12). To investigate whether Rac is also activated in Iba1- and PLC-γ-dependent membrane ruffling, the activation of Rac was monitored by pull-down assay with the Cdc42/Rac interactive binding domain of PAK (19) using PAE transfectants. In the absence of Iba1, PDGF stimulation efficiently converted Rac into the GTP-bound form in the cells expressing WT and the Y740/51 mutant but not in the cells expressing the Tyr-1021 (Fig. 5*A*), Tyr-771, or Tyr-1009 (data not shown) mutant. All lysates contained equal amounts of total Rac. These results indicate that Rac was activated through the PI3K-dependent pathway in the absence of Iba1. However, in the presence of Iba1, in addition to WT- or Y740/51-expressing cells, Tyr-1021-expressing cells also showed Rac activation in response to PDGF (Fig. 5*B*). These observations indicate the existence of an Iba1- and PLC-γ-dependent Rac-activating pathway that triggers the formation of membrane ruffles.

Inhibitory Effects of PLC-γ Mutants on Iba1-dependent Membrane Ruffling and Rac Activation—To confirm the involvement of PLC-γ in Iba1-dependent and PI3K-independent Rac activation, we investigated the effects of PLC-γ mutants that act as dominant negative forms against endogenous PLC-γ. PLC-γ1-Y771F/Y783F had phenylalanines substituted for ty-

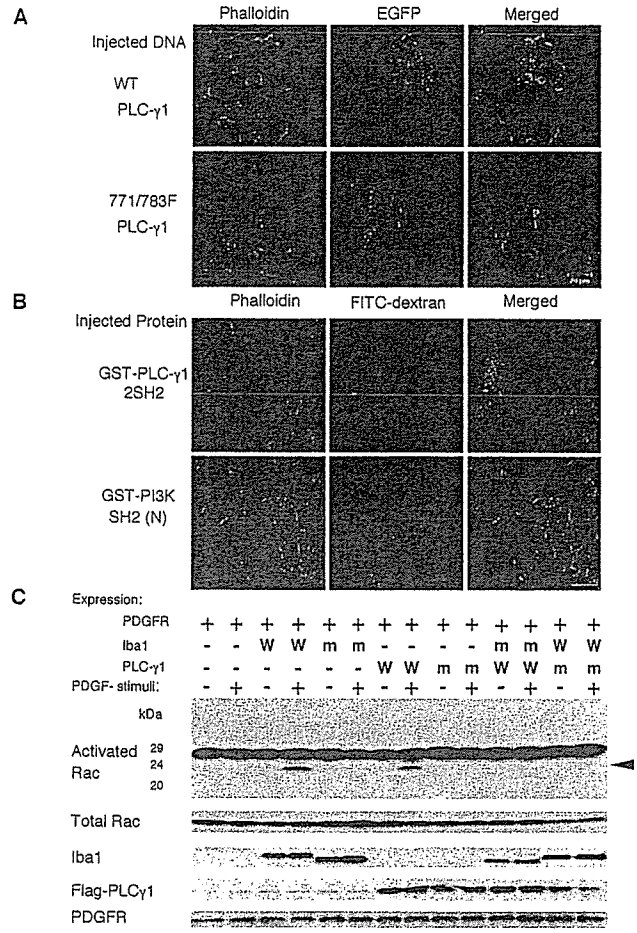

FIG. 6. **Inhibitory effects of PLC-γ mutants on membrane ruffling and Rac activation.** *A*, serum-starved Iba1- and Tyr-1021 PDGFR-expressing PAE cells were microinjected into the nucleus with pFLAG-CMV2 carrying WT or Y771F/Y783F *PLC-γ1* cDNA together with pEGFP-C1, and incubated for 3 h to induce protein expression. *B*, serum-starved Iba1- and Tyr-1021 PDGFR-expressing PAE cells were microinjected into the cytosol with GST-PLC-γ1–2SH2 or GST-PI3K SH2 (N) fusion proteins together with FITC-dextran and incubated for 10 min. Both types of cells were stimulated with 50 ng/ml PDGF for 5 min, fixed, and stained with Texas Red-phalloidin (*A* and *B*, *left panels*). Injected cells were located by fluorescence of epidermal growth factor protein and FITC-dextran (*A* and *B*, *mid panels*). *Scale bar*, 20 μm. *C*, CHO cells expressing PDGFR, and WT (*W*) or mutant (*m*) of Iba1 and FLAG-tagged PLC-γ1 were stimulated with 50 ng/ml PDGF for 2 min, lysed, and examined by GST-PAK pull-down assay, as shown in Fig. 5. Rac1, Iba1, PLC-γ1, and PDGFR in cell lysates were identified by Western blotting with anti-Rac1, anti-Iba1, anti-FLAG, and anti-PDGFR antibodies, respectively.

rosines 771 and 783 and obtained the ability to specifically suppress the activity of endogenous PLC-γ1 (16). FLAG-tagged PLC-γ1 WT or Y771F/Y783F mutant was expressed in the PAE cells expressing both PDGFR Tyr-1021 and Iba1. Subsequently, the cells were stimulated with PDGF and stained with phalloidin. Typical membrane ruffles were formed in WT PLC-γ-expressing cells that were located by the marker signal of co-expressed EGFP (Fig. 6*A*, *upper panel*). By contrast, PDGF-induced membrane ruffling was inhibited in PLC-γ1-Y771F/Y783F-expressing cells (Fig. 6*A*, *lower panel*). When the PLC-γ1-expressing cells were located with an anti-FLAG antibody, the cells that were recognized corresponded perfectly to the EGFP-expressing cells (data not shown). GST-PLC-γ1–2SH2 is a fusion protein of GST and a PLC-γ1 fragment containing two SH2 domains but no catalytic domain and is able to specifically inhibit PLC-γ1 signaling, whereas GST-PI3K SH2 (N) contains the PI3K N-terminal SH2 domain but does not suppress PLC-γ signaling (17). Into the PAE cells expressing both PDGFR Tyr-1021 and Iba1, we microinjected GST-PLC-γ1–2SH2 or GST-PI3K SH2(N) fusion protein together with FITC-conjugated dextran to mark the cells that were injected. The cells injected with GST-PLC-γ1–2SH2 fusion protein were stimulated with PDGF and stained with phalloidin. PDGF-induced membrane ruffling was inhibited in the GST-PLC-γ1–2SH2-injected cells, whereas the cells injected with GST-PI3K SH2 (N) were not inhibited.

Next we investigated whether PLC-γ1-Y771F/Y783F mutant blocked Iba1-dependent Rac activation. We induced the transient expression of WT PDGFR, and WT or mutant Iba1 and PLC-γ1 in CHO cells, which lacked PDGFR expression (26), and then examined Rac activity by GST-PAK pull-down assay. Under the conditions we used, in CHO cells expressing PDGFR only, Rac was not activated by PDGF stimulation (Fig. 6*B*, *lanes 1* and *2*), and membrane ruffles were not formed (data not shown). In the cells expressing both Iba1 and PDGFR, Rac was activated (*lanes 3* and *4*) and membrane ruffles were formed (data not shown) in response to PDGF, indicating that CHO cells also contain the pathway exerting Iba1-dependent Rac activation. In cells expressing Iba1 and PDGFR, expression of the PLC-γ1-Y771F/Y783F mutant completely suppressed Rac activation in response to PDGF (*lanes 13* and *14*). These results indicate the specific involvement of PLC-γ in Iba1-dependent Rac activation.

When the cells expressing PDGFR and PLC-γ1 were stimulated with PDGF, Rac activation was induced (*lanes 7* and *8*), whereas this Rac activation was inhibited by additional expression of mutant Iba1-(1–115), which effectively suppresses the membrane ruffling of MG5 cells (12) (*lanes 11* and *12*). PDGF did not cause Rac activation in the cells expressing PDGFR and mutant PLC-γ1-Y771F/Y783F or mutant Iba1-(1–115) (*lanes 5*, *6*, *9*, and *10*). These results suggest a functional link between PLC-γ and Iba1 in membrane ruffling and Rac activation.

Ligand-induced Tyrosine Phosphorylation of PLC-γ—During the ligand-induced activation process, PLC-γ is known to be phosphorylated by receptor tyrosine kinases (27); thus we next analyzed the tyrosine phosphorylation of PLC-γ in response to growth factors stimulating membrane ruffling. In mammals, two types of PLC-γ are known, PLC-γ1 and PLC-γ2. As shown in Fig. 7, PAE cells selectively express PLC-γ1, whereas the microglial cell line MG5 predominantly expresses PLC-γ2. The PAE cells expressing Iba1 and WT PDGFR were stimulated with PDGF, immunoprecipitated with an anti-PLC-γ1 antibody, and immunoblotted with an anti-phosphotyrosine antibody, 4G10. Phosphorylation of PLC-γ1 was detected 30 s after PDGF stimulation, and after 2 min, the signal was greatly intensified (Fig. 7*A*). When MG5 cells were stimulated with M-CSF, phosphorylation of PLC-γ1 was, by contrast, undetectable even after 2 min. On the other hand, phosphorylation of PLC-γ2 was clearly detected in MG5 cells after M-CSF stimulation (Fig. 7*B*). These observations indicate that, in response to peptide growth factors, PLC-γ1 and - γ2 are phosphorylated in these Iba1-expressing cells, including macrophages/microglia, and exert their activity during membrane ruffling.

DISCUSSION

In our previous report (12), Iba1 was revealed to be a macrophage/microglia-specific EF hand protein responsible for M-CSF- and Rac-induced membrane ruffling. In this study, to analyze the functions of Iba1 in more detail, we introduced an Iba1 expression construct into Swiss 3T3, PAE, and CHO cells, stimulated the cells with PDGF, and examined signaling profiles leading to Rac activation and subsequent membrane ruffling. As a result, we elucidated a novel signaling pathway

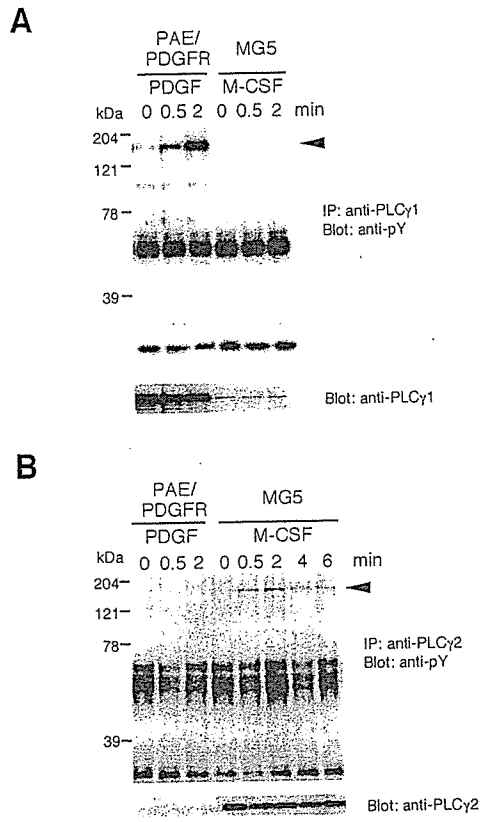

FIG. 7. **Ligand-dependent tyrosine phosphorylation of PLC-γ.** Serum-starved WT PDGFR-expressing PAE and M-CSF-starved MG5 cells were stimulated for the indicated times with or without 50 ng/ml PDGF and 100 ng/ml M-CSF, respectively. The cells were lysed and immunoprecipitated with an anti-PLC-γ1 (*A*) or anti-PLC-γ2 (*B*) antibody. Samples were subjected to Western blotting with an anti-phosphotyrosine antibody, 4G10 (*upper panels*) and sequentially reprobed with anti-PLC-γ1 (*A*) and anti-PLC-γ2 (*B*) antibodies (*lower panels*). *Arrowheads* indicate positions of PLC-γ1 and PLC-γ2.

where, in the presence of Iba1, Rac is activated in a manner dependent on PLC-γ.

In response to PDGF, Iba1-expressing Swiss 3T3 cells exhibited enhanced membrane ruffling and increased chemotactic activity in comparison with Iba1-nonexpressing Swiss 3T3 cells (Figs. 1*B* and 2). Recent experiments have suggested that PI3K plays a role in receptor tyrosine kinase-mediated membrane ruffling and chemotaxis in many types of cells (24, 25, 28–30). Among them, in Swiss 3T3 and PAE cells, PI3K is reported to be exclusively responsible for Rac activation (24, 25, 31, 32). Indeed, treatment with wortmannin or LY294002 effectively suppressed the PDGF-induced membrane ruffling of Iba1-nonexpressing Swiss 3T3 cells (Fig. 3). In addition, in the absence of Iba1, PDGF could not induce Rac activation and membrane ruffling in PAE cells expressing PDGFR mutants incapable of activating of PI3K (Fig. 4 and 5*A*). By contrast, membrane ruffling of Iba1-expressing Swiss 3T3 cells was not significantly inhibited by wortmannin or LY294002 (Fig. 3). Furthermore, in the presence of Iba1, PDGF stimulation actually induced Rac activation and membrane ruffling in PAE cells expressing the PDGFR mutant that is capable of activating PLC-γ but not PI3K (Figs. 4 and 5). These findings indicate the existence of an Iba1-dependent, PI3K-independent pathway leading to Rac activation and membrane ruffling, and suggest the involvement of PLC-γ in this pathway. In fact, dominant negative forms of PLC-γ clearly inhibited Iba1-dependent membrane ruffling (Fig. 6, *A* and *B*) and Rac activation (Fig. 6*C*). PLC-γ was further shown to be phosphorylated during membrane ruffling (Fig. 7). These observations indicate that PLC-γ is specifically involved in Iba1-dependent Rac activation and membrane ruffling and that Iba1 is the molecule responsible for connecting the signaling pathways of Rac and PLC-γ.

Recent studies have provided increased evidence for PI3K-independent Rac activation. Wortmannin-treated macrophages still induced ruffling at the dorsal surface after M-CSF stimulation (33). *N*-Formyl-Met-Leu-Phe induced wortmannin- and LY294002-resistant Rac activation in neutrophils (34–36). In our studies, pretreatment with wortmannin did not block M-CSF-induced membrane ruffling of microglial cell line MG5 and primarily cultured microglia (data not shown). These observations strongly suggest the existence of a PI3K-independent pathway leading to Rac activation and membrane ruffling. Kundra *et al.* (37) showed that the mutant PDGFR, which lacks the binding site for PLC-γ, could not transduce chemotactic signals when expressed in TRMP cells. Expression of another PDGFR mutant that induces increased PLC-γ activation by PDGF showed increased chemotactic activity in PAE cells (31). It is probable that PI3K and/or PLC-γ are required for chemotaxis by PDGFR. Hashimoto *et al.* (38) reported that both PLC-γ and Rac are involved in B cell antigen receptor-induced activation of MAP kinases, suggesting that PLC-γ and Rac are able to work cooperatively in a common signaling process. However, to date, the molecules that link PLC-γ and Rac pathways have been completely unknown. Iba1 or unknown Iba1-related molecules should, at least in part, underlie PI3K-independent, PLC-γ-dependent pathways that induce Rac activation.

CHO cells expressing PDGFR did not respond to PDGF in Rac activation; however, overexpression of PLC-γ induced Rac activation in response to PDGF (Fig. 6*C*). Furthermore, once-promoted Rac activation was suppressed by additional expression of a repressive mutant of Iba1. In conjunction with the parallel results shown with mutant PLC-γ and WT Iba1, the functions of Iba1 and PLC-γ in Rac activation are considered to be closely related. It is likely that Iba1 may modulate the PLC-γ-dependent signaling pathway. During membrane ruffling, complicated machineries are constructed by Iba1, PLC-γ, and other signaling molecules, including Rac, which co-operate in interactions between each them. However, unfortunately, we have no clear evidence to demonstrate direct binding among Iba1, PLC-γ, and Rac. We are now investigating conditions that would support their association.

Activated PLC-γ translocates to the inside surface of the cell membrane and catalyzes the hydrolysis of phosphatidylinositol 4,5-bisphosphate to form diacylglycerol and inositol 1,4,5-trisphosphate, which are capable of activating protein kinase C (PKC) and mobilizing intracellular calcium ($[Ca^{2+}]_i$), respectively. In our preliminary experiments, membrane ruffling of Iba1-expressing Swiss 3T3 cells was not suppressed by pretreatment with phorbol ester to down-regulate PKC (data not shown). On the other hand, M-CSF-induced membrane ruffling of MG5 cells was accompanied by $[Ca^{2+}]_i$ spikes and was completely inhibited by chelation of cytoplasmic free calcium with *O,O'*-Bis(2-aminophenyl)ethylene glycol-*N,N,N',N'*-tetraacetic acid, tetraacetoxyethyl ester (12). Iba1 actually possesses calcium-binding activity; furthermore, an Iba1 mutant without calcium-binding activity suppressed M-CSF-induced membrane ruffling (12). Several pieces of evidence indicate the significance of calcium signaling in actin remodeling (3, 39). These observations point to the importance of $[Ca^{2+}]_i$ in Iba1-related membrane ruffling and suggest that $[Ca^{2+}]_i$ mobilization is a strong candidate for linking PLC-γ and Iba1 molecules.

Iba1 also translocates to the cell membrane during mem-

brane ruffling (12). In our preliminary studies, Iba1 was demonstrated to bind to phosphatidylserine in the presence of calcium (data not shown), suggesting that Iba1 translocates to the phosphatidylserine-rich inner surface of the cell membrane in a calcium-dependent manner. Iba1 was further shown to bind to phosphatidylinositol 4,5-bisphosphate, the significant substrate of PLC-γ. Iba1 may, directly or indirectly, support translocation of PLC-γ to the cell membrane and its substrate, and may induce Rac activation by potentiating the activity of PLC-γ. Indeed, overexpression of PLC-γ in CHO cells enhanced activation of Rac (Fig. 6*C*). Although it seems rather inconsistent with data presented here, mutant Iba1 suppressed membrane ruffling induced by activated RacV12 in our previous paper (12). Preliminarily, mutant Iba1 exhibited loss of ability to translocate, localized constitutively to the cell membrane, and disrupted surrounding actin architecture (data not shown). RacV12 showed a tendency to be excluded from the site where mutant Iba1 accumulated (data not shown). In our hypothesis, Iba1 may also function in translocation of Rac, and mutant Iba1 may suppress membrane ruffling by inhibiting appropriate translocation of RacV12.

Macrophages are extremely motile. To express this phenotype, macrophages have to contain highly integrated mechanisms that regulate dynamic reorganization of the actin cytoskeleton. In addition to the well-known PI3K-organized Rac regulation, Iba1- and PLC-γ-based mechanisms are likely to direct Rac activity in macrophages. Herein, we have shown direct evidence that PLC-γ activates Rac and causes membrane ruffling in the presence of Iba1. This finding indicates that macrophages/microglia have at least dual control pathways to regulate Rac activity and exert extreme motile activity by these systems. In fact, some studies suggest cross-talk between PI3K and PLC-γ pathways (31, 40, 41). Iba1 is therefore considered to be a crucial molecule for the function of activated macrophages/microglia. Further studies are definitely required to determine the precise molecular mechanisms underlying Iba1- and PLC-γ-dependent activation of Rac and membrane ruffling.

Acknowledgments—We thank Dr. Carl-Henrik Heldin (Ludwig Institute for Cancer Research) and Dr. Koutaro Yokote (Chiba University) for providing us with PAE cells, Dr. Andrius Kazlauskas (Harvard Medical School) for pLXSN plasmids carrying the human WT or mutant β-PDGFRs, Dr. Pann-Ghill Suh (Pohang University of Science and Technology) for pFLAG-CMV2 plasmids carrying the WT or mutant PLC-γ1, and Dr. Tadaomi Takenawa and Dr. Kiyoko Fukami (Institute of Medical Science, University of Tokyo) for expression plasmids of GST-PLCγ1–2SH2 and GST-PI3-K SH2(N). We also thank Dr. Koutaro Yokote and Dr. Kiyoko Fukami for helpful discussion.

REFERENCES

1. Stossel, T. P. (1993) *Science* **260,** 1086–1094
2. Mitchison, T. J., and Cramer, L. P. (1996) *Cell* **84,** 371–379
3. Hartwig, J. H., and Yin, H. L. (1988) *Cell Motil. Cytoskeleton* **10,** 117–125
4. Downey, G. P. (1994) *Curr. Opin. Immunol.* **6,** 113–124
5. Nakajima, K., and Kohsaka, S. (1993) *Neurosci. Res.* **7,** 187–203
6. Kreutzberg, G. W. (1996) *Trends Neurosci.* **19,** 312–318
7. Hall, A. (1998) *Science* **279,** 509–514
8. Ridley, A. J., Paterson, H. F., Johnston, C. L., Diekmann, D., and Hall, A. (1992) *Cell* **70,** 401–410
9. Imai, Y., Ibata, I., Ito, D., Ohsawa, K., and Kohsaka, S. (1996) *Biochem. Biophys. Res. Commun.* **224,** 855–862
10. Ito, D., Imai, Y., Ohsawa, K., Nakajima, K., Fukuuchi, Y., and Kohsaka, S. (1998) *Brain Res. Mol. Brain Res.* **57,** 1–9
11. Ohsawa, K., Imai, Y., Nakajima, K., and Kohsaka, S. (1997) *Glia* **21,** 285–298
12. Ohsawa, K., Imai, Y., Kanazawa, H., Sasaki, Y., and Kohsaka, S. (2000) *J. Cell Sci.* **113,** 3073–3084
13. Allen, W. E., Jones, G. E., Pollard, J. W., and Ridley, A. J. (1997) *J. Cell Sci.* **110,** 707–720
14. Westermark, B., Siegbahn, A., Heldin, C.-H., and Claesson-Welsh, L. (1990) *Proc. Natl. Acad. Sci. U. S. A.* **87,** 128–132
15. Valius, M., and Kazlauskas, A. (1993) *Cell* **73,** 321–334
16. Kim, H. K., Kim, J. W., Zilberstein, A., Margolis, B., Kim, J. G., Schlessinger, J., and Rhee, S. G. (1991) *Cell* **65,** 435–441
17. Homma, Y., and Takenawa, T. (1992) *J. Biol. Chem.* **267,** 21844–21849
18. Yokote, K., Mori, S., Siegbahn, A., Rönnstrand, L., Wernstedt, C., Heldin, C.-H., and Claesson-Welsh, L. (1996) *J. Biol. Chem.* **271,** 5101–5111
19. Manser, E., Loo, T.-H., Koh, C.-G., Zhao, Z.-S., Chen, X.-Q., Tan, L., Tan, I., Leung, T., and Lim, L. (1998) *Mol. Cell* **1,** 183–192
20. Ridley, A. J., and Hall, A. (1992) *Cell* **70,** 389–399
21. Kozma, R., Ahmed, S., Best, A., and Lim, L. (1995) *Mol. Cell. Biol.* **15,** 1942–1952
22. Nobes, C. D., and Hall, A. (1995) *Cell* **81,** 53–62
23. Sánchez-Madrid, F., and del Pozo, M. A. (1999) *EMBO J.* **18,** 501–511
24. Nobes, C. D., Hawkins, P., Stephens, L., and Hall, A. (1995) *J. Cell Sci.* **108,** 225–233
25. Wennström, S., Siegbahn, A., Yokote, K., Arvidsson, A.-K., Heldin, C.-H., Mori, S., and Claesson-Welsh, L. (1994) *Oncogene* **9,** 651–660
26. Ma, Y.-H., Reusch, H. P., Wilson, E., Escobedo, J. A., Fantl, W. J., Williams, L. T., and Ives, H. E. (1994) *J. Biol. Chem.* **269,** 30734–30739
27. Mustelin, T., Coggeshall, K. M., Isakov, N., and Altman, A. (1990) *Science* **247,** 1584–1587
28. Kotani, K., Yonezawa, K., Hara, K., Ueda, H., Kitamura, Y., Sakaue, H., Ando, A., Chavanieu, A., Calas, B., Grigorescu, F., Nishiyama, M., Waterfield, M. D., and Kasuga, M. (1994) *EMBO J.* **13,** 2313–2321
29. Arrieumerlou, C., Donnadieu, E., Brennan, P., Keryer, G., Bismuth, G., Cantrell, D., and Trautmann, A. (1998) *Eur. J. Immunol.* **28,** 1877–1885
30. Hooshmand-Rad, R., Claesson-Welsh, L., Wennström, S., Yokote, K., Siegbahn, A., and Heldin, C.-H. (1997) *Exp. Cell Res.* **234,** 434–441
31. Rönnstrand, L., Siegbahn, A., Rorsman, C., Johnell, M., Hansen, K., and Heldin, C.-H. (1999) *J. Biol. Chem.* **274,** 22089–22094
32. Hawkins, P. T., Eguinoa, A., Qiu, R.-G., Stokoe, D., Cooke, F. T., Walters, R., Wennström, S., Claesson-Welsh, L., Evans, T., Symons, M., and Stephens, L. (1995) *Curr. Biol.* **5,** 393–403
33. Araki, N., Johnson, M. T., and Swanson, J. A. (1996) *J. Cell Biol.* **135,** 1249–1260
34. Benard, V., Bohl, B. P., and Bokoch, G. M. (1999) *J. Biol. Chem.* **274,** 13198–13204
35. Akasaki, T., Koga, H., and Sumimoto, H. (1999) *J. Biol. Chem.* **274,** 18055–18059
36. Geijsen, N., van Delft, S., Raaijmakers, J. A. M., Lammers, J.-W., Collard, J. G., Koenderman, L., and Coffer, P. J. (1999) *Blood* **94,** 1121–1130
37. Kundra, V., Escobedo, J. A., Kazlauskas, A., Kim, H. K., Rhee, S. G., Williams, L. T., and Zetter, B. R. (1994) *Nature* **367,** 474–476
38. Hashimoto, A., Okada, H., Jiang, A., Kurosaki, M., Greenberg, S., Clark, E. A., and Kurosaki, T. (1998) *J. Exp. Med.* **188,** 1287–1295
39. Janmey, P. A. (1994) *Annu. Rev. Physiol.* **56,** 169–191
40. Bae, Y. S., Cantley, L. G., Chen, C. S., Kim, S. R., Kwon, K. S., and Rhee, S. G. (1998) *J. Biol. Chem.* **273,** 4465–4469
41. Falasca, M., Logan, S. K., Lehto, V. P., Baccante, G., Lemmon, M. A., and Schlessinger, J. (1998) *EMBO J.* **17,** 414–422

Available online at www.sciencedirect.com
SCIENCE DIRECT®
Life Sciences 72 (2002) 431–442
ELSEVIER
Life Sciences
www.elsevier.com/locate/lifescie

Spatial and temporal aspects of Ca^{2+} signaling mediated by P2Y receptors in cultured rat hippocampal astrocytes

Schuichi Koizumi[a,*], Yoshiro Saito[b], Ken Nakazawa[a], Kazuyuki Nakajima[c], Jun-Ichi Sawada[b], Shinichi Kohsaka[c], Peter Illes[d], Kazuhide Inoue[a]

[a] *Division of Pharmacology, National Institute of Health Sciences, 1-18-1 Kamiyoga, Setagaya, Tokyo 158, Japan*
[b] *Division of Biochemistry and Immunochemistry, National Institute of Health Sciences, 1-18-1 Kamiyoga, Setagaya, Tokyo 158-8501, Japan*
[c] *Department of Neurochemistry, National Institute of Neuroscience, 4-1-1 Ogawa-higashi, Kodaira, Tokyo 187-8502, Japan*
[d] *Department of Pharmacology and Toxicology, University of Leipzig, D-04107 Leipzig, Germany*

Abstract

ATP produces a variety of Ca^{2+} responses in astrocytes. To address the complex spatio-temporal Ca^{2+} signals, we analyzed the ATP-evoked increase in intracellular Ca^{2+} concentration ($[Ca^{2+}]i$) in cultured rat hippocampal astrocytes using fura-2 or fluo-3 based Ca^{2+} imaging techniques. ATP at less than 10 nM produced elementary Ca^{2+} release event "puffs" in a manner independent of extracellular Ca^{2+}. Stimulation with higher ATP concentrations (3 or 10 μM) resulted in global Ca^{2+} responses such as intercellular Ca^{2+} wave. These Ca^{2+} responses were mainly mediated by metabotropic P2Y receptors. ATP acting on both P2Y1 and P2Y2 receptors produced a transient Ca^{2+} release by inositol 1,4,5-trisphosphate ($InsP_3$). When cells were stimulated with ATP much longer, the transient $[Ca^{2+}]i$ elevation was followed by sustained Ca^{2+} entry from the extracellular space. This sustained rise in $[Ca^{2+}]i$ was inhibited by Zn^{2+} (< 10 μM), an inhibitor of capacitative Ca^{2+} entry (CCE). CCE induced by cyclopiazonic acid or thapsigargin and Ca^{2+} entry evoked by ATP share the same pharmacological profile in astrocytes. Taken together, the hierarchical Ca^{2+} responses to ATP were observed in hippocampal astrocytes, i.e., puffs, global Ca^{2+} release by $InsP_3$, and CCE in response to depletion of $InsP_3$-sensitive Ca^{2+} stores. It should be noted that these Ca^{2+} signals and their modulation by Zn^{2+} could occur in the hippocampus *in situ* since both ATP and Zn^{2+} are rich in the hippocampus and could be released by excitatory stimulation.

Keywords: ATP; Elementary Ca^{2+} events; Puffs; Capacitative Ca^{2+} entry; Zn^{2+}; Hippocampal astrocytes; P2Y receptor

* Corresponding author. Tel./fax: +81-3-3700-9698.
E-mail address: skoizumi@nihs.go.jp (S. Koizumi).

0024-3205/02/$ - see front matter © 2002 Elsevier Science Inc. All rights reserved.
PII: S0024-3205(02)02273-7

Introduction

Glial cells respond to variety of stimuli such as neurotransmitters or hormones, and show complex changes in intracellular Ca^{2+} concentration ($[Ca^{2+}]i$). ATP at relatively low concentrations has been reported to promote large Ca^{2+} signals in almost all types of glial cells [12,21]. In addition, it is reported that ATP is released from both neurons [22,9] and astrocytes [7] by excitatory stimulation or mechanical stimulation, respectively. Thus, ATP would function as an important intercellular messenger to form complex Ca^{2+} signals in astrocytes in the CNS. Although endogenous release of ATP might be very small and localized, such a low ATP concentration could produce highly localized Ca^{2+} release events such as "puffs", a local Ca^{2+} release event through a cluster of inositol 1,4,5-trisphosphate receptors ($InsP_3Rs$) [3,16]. Puffs arise from discrete sites at low $InsP_3$ levels and become coordinated at higher $InsP_3$ levels to produce global $[Ca^{2+}]i$ elevation or a Ca^{2+} wave. The hierarchical organization of Ca^{2+} release from intracellular Ca^{2+} stores ranging from Ca^{2+} puffs to larger subcellular events and ultimately to global Ca^{2+} waves suggests that cells can use considerable flexibility in the temporal and spatial pattern of a Ca^{2+} response. However, such localized Ca^{2+} signals in astrocytes are not fully clarified.

It is also controversial as to whether glial cells possess "capacitative Ca^{2+} entry" (CCE), Ca^{2+} entry activated by depletion of internal Ca^{2+} stores [18]. Although the mechanism underlying CCE has not been deduced, it has become clear that CCE is activated by activation of receptors linked to $InsP_3$ formation and has an important role in many aspects of intracellular signaling in non-excitable cells [2] and even in excitable cells [4]. A transient $[Ca^{2+}]i$ increase followed by sustained Ca^{2+} entry has been seen in enteric glia [11], oligodendrocytes [20], and astrocytes [10]. However, current reports on ATP-evoked changes of $[Ca^{2+}]i$ in glial cells are somewhat contradictory.

In the present study, we focused on astrocytic puffs and CCE evoked by ATP and demonstrate that ATP at a very low concentration (10 nM) stimulates phospholipase $C\beta/InsP_3$ coupled P2Y receptors resulting in localized Ca^{2+} signals, i.e., puffs. Puffs become coordinated at higher $InsP_3$ levels to produce a global $[Ca^{2+}]i$ elevation or Ca^{2+} wave. The sustained $InsP_3$ levels by higher ATP caused a sustained Zn^{2+}-sensitive Ca^{2+} entry, probably CCE. Astrocytes may use such hierarchical Ca^{2+} signals to process complex information.

Methods

Cell culture

Hippocampal cortices were dissected from newborn Wistar rats (1 day), and were minced and treated with papain (9 U/mL; Worthngton Biochemical, Freedhold, NJ, U.S.A.). After enzyme treatment at 37 °C for 10 min, cells were dispersed by gentle agitation through a pipette and were plated in a flask. For purification of astrocytes, the flask was shook for 12 h one week after seeding. The cells were plated again in a flask and cultured, then cells were seeded on poly-L-lysine-coated glass coverslips with a silicon rubber wall (Flexiperm, Heraeus Biotechnology, Hanau, Germany) at a density of 2×10^5 cells/cm^2. For measurement of $InsP_3$ formation, the cells were plated on poly-L-lysine-coated plastic 24-well culture plates (Falcon, Becton Dickinson Company, Lincoln Park, NJ, U.S.A.) at the same density as mentioned above.

Measurement of $[Ca^{2+}]i$ in single cells

The increase in $[Ca^{2+}]i$ in single cells was measured by the fura-2 method with minor modifications [14]. The cells were washed with balanced salt solution (BSS) of the following composition (in mM): NaCl 150, KCl 5.0, $CaCl_2$ 1.2, $MgCl_2$ 1.2, N-2-hydroxyethylpiperazine-N′ -2-ethanesulfonic acid (HEPES) 25, and D-glucose 10, and incubated with 5 μM fura-2 acetoxymethylester (fura-2 AM) at 37 °C in BSS. The coverslips were mounted on an inverted epifluorescence microscope (TMD-300, Nikon, Tokyo, Japan) equipped with a 75 W xenon-lamp and band-pass filters of 340 nm wavelength for measurement of the Ca^{2+}-dependent signal (F340) and 360 nm wavelength for measurement of the Ca^{2+}-independent signal (F360).

Confocal Ca^{2+} imaging

For recording subcellular Ca^{2+} signals, the cells were loaded with 5 μM fluo-3 or fluo-4AM for 30–40 min at room temperature. After a further 20–30 min for de-esterification of the acetoxymethyl ester, the coverslips were mounted on a microscope (E-600, Nikon, Tokyo, Japan) equipped with CSU-10 laser-scanning unit (Yokogawa, Tokyo, Japan) and ICCD camera (C2400-87V, Hamamatsu Photonics, Japan). Fluo-3 or fluo-4 was excited with the 488 nm line of an argon–ion laser and the emitted fluorescence was collected at wavelengths >515 nm.

Measurement of $InsP_3$ concentration

Assay of $InsP_3$ formation was performed by radioreceptor assay using an $InsP_3$ assay kit (TRK 1000, Amersham, Bucks, UK). Cells were stimulated with various concentrations of ATP or its analogues for 30 s. After termination by the addition of 0.2 volumes ice-cold 20% $HClO_4$, cells were homogenized, transferred, and then centrifuged. Supernatants were neutralized to pH 7.5 by 1.5 M KOH. Precipitated $KClO_4$ was sedimented by centrifugation (12000 × g for 15 min at 4 °C) and removed, and then the supernatants were used for radioreceptor assay of $InsP_3$.

Statistics

All the data are mean ± s.e.m. Statistical differences in the value of the increase in $[Ca^{2+}]i$ was determined using an analysis of variance followed by Dunnet's test for multiple comparisons.

Results

Ca^{2+} puffs in astrocytes

Almost all cells were positive to an anti-GFAP antibody, showing that these cells are astrocytes. Using a confocal Ca^{2+} imaging system, elementary Ca^{2+} events were investigated. Elementary Ca^{2+} events were observed spontaneously and were facilitated upon stimulation with lower ATP concentrations (~ 10 nM) that were sub-threshold for global Ca^{2+} signaling. The number of events in the absence and presence of ATP (10 nM) was 1.5 ± 0.12 and 3.7 ± 0.22 (/cell, $p < 0.01$),

respectively. The spatially restricted Ca^{2+} signals evoked by 10 nM ATP were observed in the majority of cells (78%, n = 79) (Fig. 1, trace 2 and image b). These Ca^{2+} signals were brief events that propagated only short distances, and were similar to so-called "Ca^{2+} puffs." Such elementary signals occurred at various locations. The elementary Ca^{2+} release sites appeared to be differentially active, with some displaying multiple events (trace 2), while another showed a lower activity (trace 1). Repeated application of ATP triggered elementary Ca^{2+} signals at the same locations (data not shown). Application of 10 μM ATP resulted in global $[Ca^{2+}]i$ increase. The elementary Ca^{2+} signals were observed in the absence of extracellular Ca^{2+}, but abolished by U73122 (1 μM, 10 min), an inhibitor of phospholipase C (PLC), suggesting that ATP causes Ca^{2+} release by activating metabotropic P2Y receptors.

Pharmacological analysis of ATP-evoked global $[Ca^{2+}]i$ elevation in astrocytes

Using a fura-2 method, ATP-, its analogues-, and UTP-evoked rises in $[Ca^{2+}]i$ were investigated in hippocampal astrocytes. Values of ED50 for 2MeSATP, ADP, ATP, ATPγS, and UTP were 0.3, 2, 3, 10,

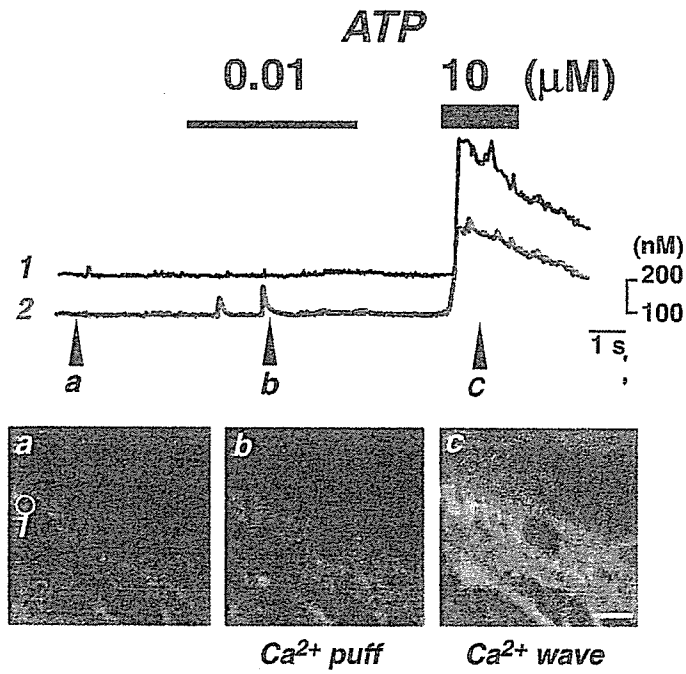

Fig. 1. From elementary Ca^{2+} release to global Ca^{2+} response in hippocampal astrocytes. When astrocytes were stimulated with a lower ATP concentration (10 nM), spatially and temporally restricted Ca^{2+} release events (puffs) were observed in the majority of astrocytes (trace 2 and panel b). Application of a higher ATP concentration (10 μM) resulted in a global Ca^{2+} wave in almost all astrocytes (panel c). Such elementary Ca^{2+} release events were observed even in the absence of extracellular Ca^{2+}, but were abolished by U73122 (1 μM, 10 min).

and 30 μM, respectively (Fig. 2). These responses were not blocked by the treatment of cells with PTX (data not shown). Glutamate (10 μM) also produced a rise in $[Ca^{2+}]i$ which was inhibited by CNQX (30 μM) in the cells. However, the ATP-evoked elevation in $[Ca^{2+}]i$ was unaffected by CNQX (data not shown).

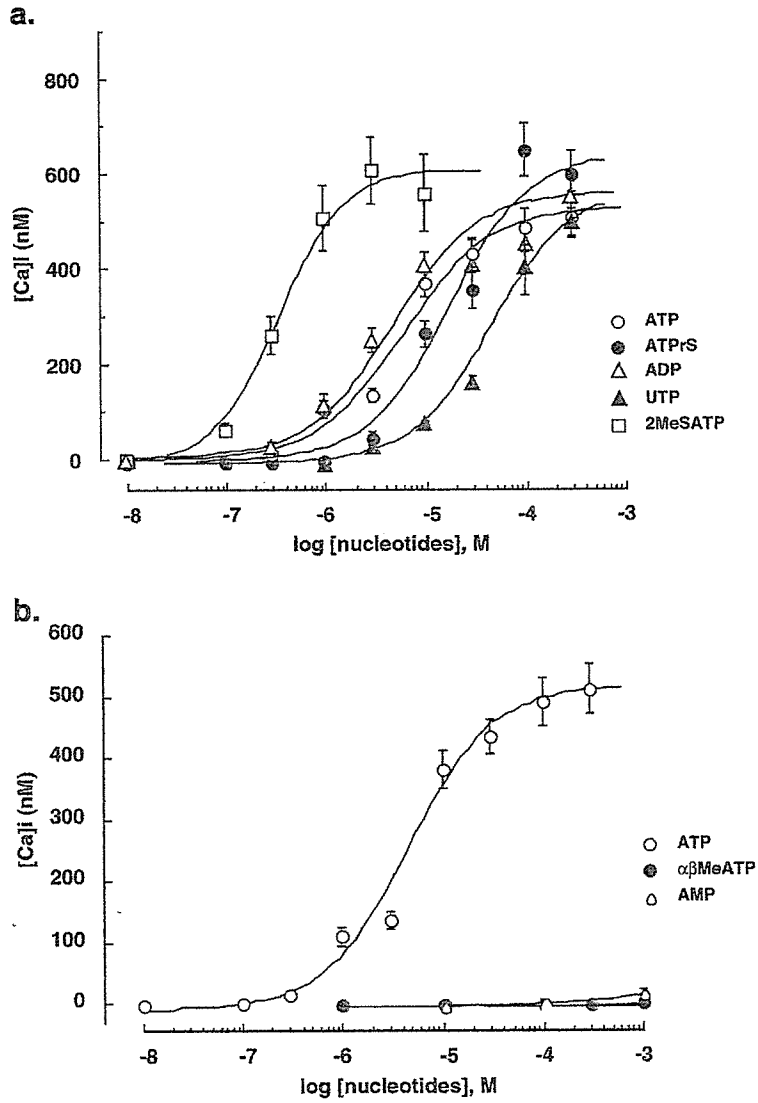

Fig. 2. Concentration-dependence curves for ATP, its analogues, and UTP in stimulating the increase in $[Ca^{2+}]i$ in hippocampal astrocytes. These reagents were applied to the cells for 15 s and the maximal responses above basal levels of $[Ca^{2+}]i$ are shown. Each symbol represents mean ± s.e.m. from 16–64 cells tested. In A, open circles, closed circles, open triangles, closed triangles, and open squares show ATP, ATPγS, ADP, UTP, and 2MeSATP, respectively. In B, open circles, closed circles, open triangles, and closed triangles show ATP, αβ-MeATP, AMP, and adenosine, respectively.

Effects of nicardipine, Cd^{2+}, Zn^{2+}, and Ca^{2+}-depletion on the ATP-evoked $[Ca^{2+}]i$ rise

ATP (3 μM) was applied to the cells twice for 10 s separated by 2 min and the first and the second responses to ATP were defined as S1 and S2, respectively. The first treatment was always made with ATP alone and the second treatment was made under various conditions (Fig. 3). The S2/S1 ratio (S2/S1) was calculated and adopted as an index to compare the data among different cells. In the control

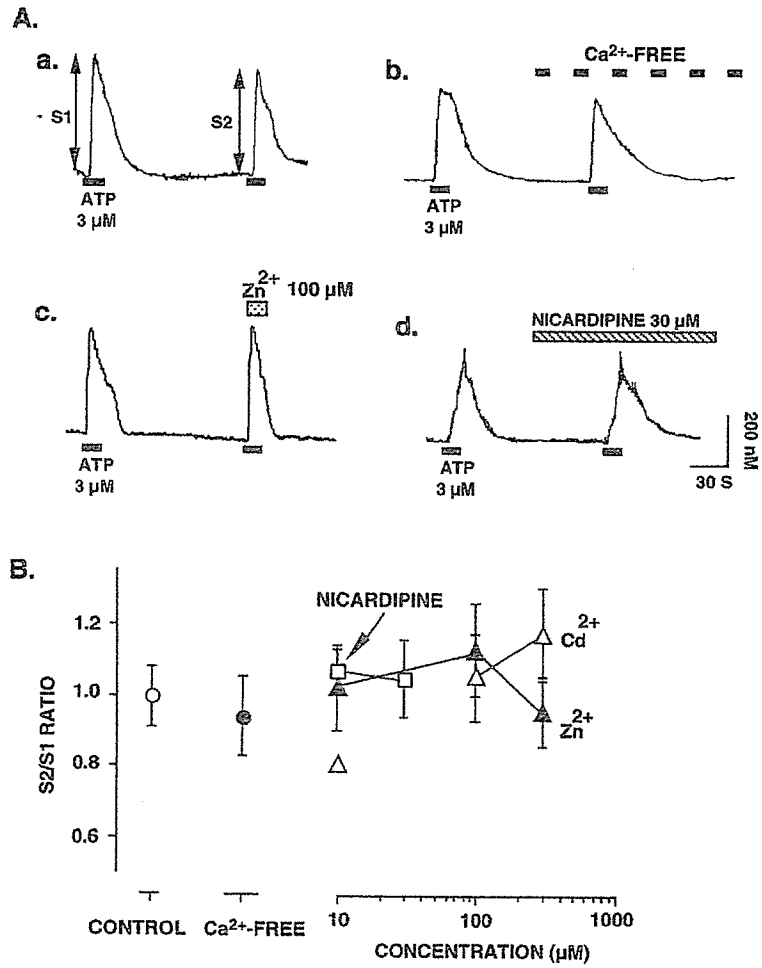

Fig. 3. The effects of nicardipine Cd^{2+}, Zn^{2+}, and Ca^{2+}-depletion on the ATP-evoked increase in $[Ca^{2+}]i$ in hippocampal astrocytes. A-a, ATP was applied to the cells twice for 15 s separated by 2 min (solid bars) and the first and the second responses to ATP were defined as S1 and S2, respectively. b, Thirty seconds after the first ATP-application in Ca^{2+}-containing medium, the cells were perfused with Ca^{2+}-free BSS for 2 min, and then the second ATP was applied to the cells in the solution. c, The effects of nicardipine (30 μM) on the ATP-evoked rise in $[Ca^{2+}]i$. Nicardipine was applied to the cells 30 s before and during the second ATP-application. B, Summary of the effects of nicardipine, Cd^{2+}, Zn^{2+}, and Ca^{2+}-depletion on the ATP-evoked $[Ca^{2+}]i$ rise. Values show the S2/S1 ratio. The data are mean ± s.e.m. from 22 (ATP alone), 51 (Ca^{2+}-FREE), 25 (nicardipine), 16 (Cd^{2+}), and 17–25 (Zn^{2+}; 10–300 μM) cells tested. Cd^{2+} or Zn^{2+} were applied to the cells only during the second ATP-application.

experiment, the S2/S1 ratio was 1.0 ± 0.09 (n = 22) (Fig. 3A-a), which was unaffected by Ca^{2+}-free BSS (Fig. 3B). ATP analogues and UTP (0.3–30 μM) also caused an increase in $[Ca^{2+}]i$ of a similar magnitude in the absence of external Ca^{2+} (data not shown). Nicardipine (30 μM) or Cd^{2+} (100 μM), antagonists to voltage-gated Ca^{2+} channels and Zn^{2+} (0.1–10 μM), which is known to facilitate Ca^{2+} influx through channel forming P2X receptors [14], but is known to inhibit Ca^{2+} influx mediated by metabotropic P2Y receptors [13], had no effect on the Ca^{2+} response (Fig. 3A-c and B).

ATP-evoked formation of $InsP_3$

Changes in intracellular $InsP_3$ concentration evoked by ATP were investigated. The resting level of $InsP_3$ was 3.0 pmol/well (n = 2). ATP stimulated the formation of $InsP_3$ in a concentration dependent manner over a concentration range from 1 to 30 μM and, at 30 μM, increased the $InsP_3$ concentration to 15.5 pmol/well (n = 2) (Fig. 4). The ED50 value was approximately 3 μM (Fig. 4). 2MeSATP (3 μM) and UTP (30 μM) also produced a rise in intracellular $InsP_3$, but αβ-MeATP (100 μM) did not. Suramin (100 μM) abolished the $InsP_3$ formation evoked by ATP.

Sustained Ca^{2+} entry by ATP in hippocampal astrocytes

As shown in Fig. 5, when ATP was applied to cells for 1 min, ATP produced a transient $[Ca^{2+}]i$ followed by a more sustained one in the presence of external Ca^{2+} in an extracellular Ca^{2+}-dependent

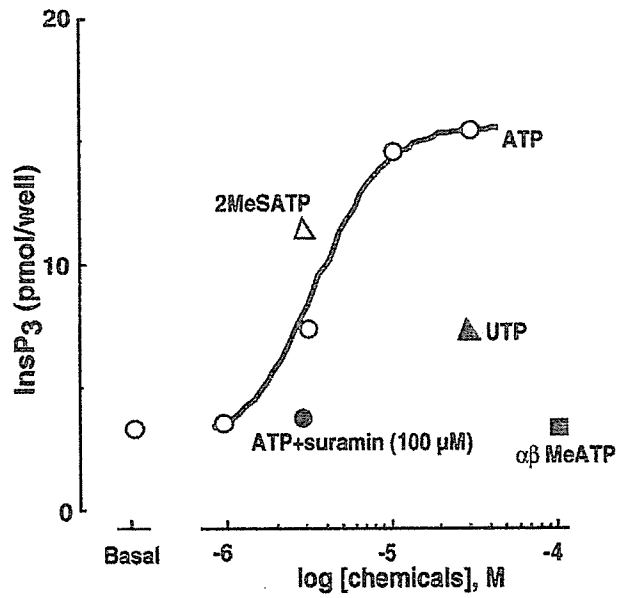

Fig. 4. Concentration-dependence of $InsP_3$ formation evoked by ATP and its analogues and UTP in hippocampal astrocytes. The open circles, triangle, closed triangle, and open square show the responses evoked by ATP, 2MeSATP, UTP, and αβ-MeATP, respectively. These are results from a typical experiment with each data point being the mean of duplicate measurements. The closed circle indicates the response evoked by 3 μM ATP in the presence of 100 μM suramin. Values show the amount of $InsP_3$ (pmol/well). Three such experiments were performed.

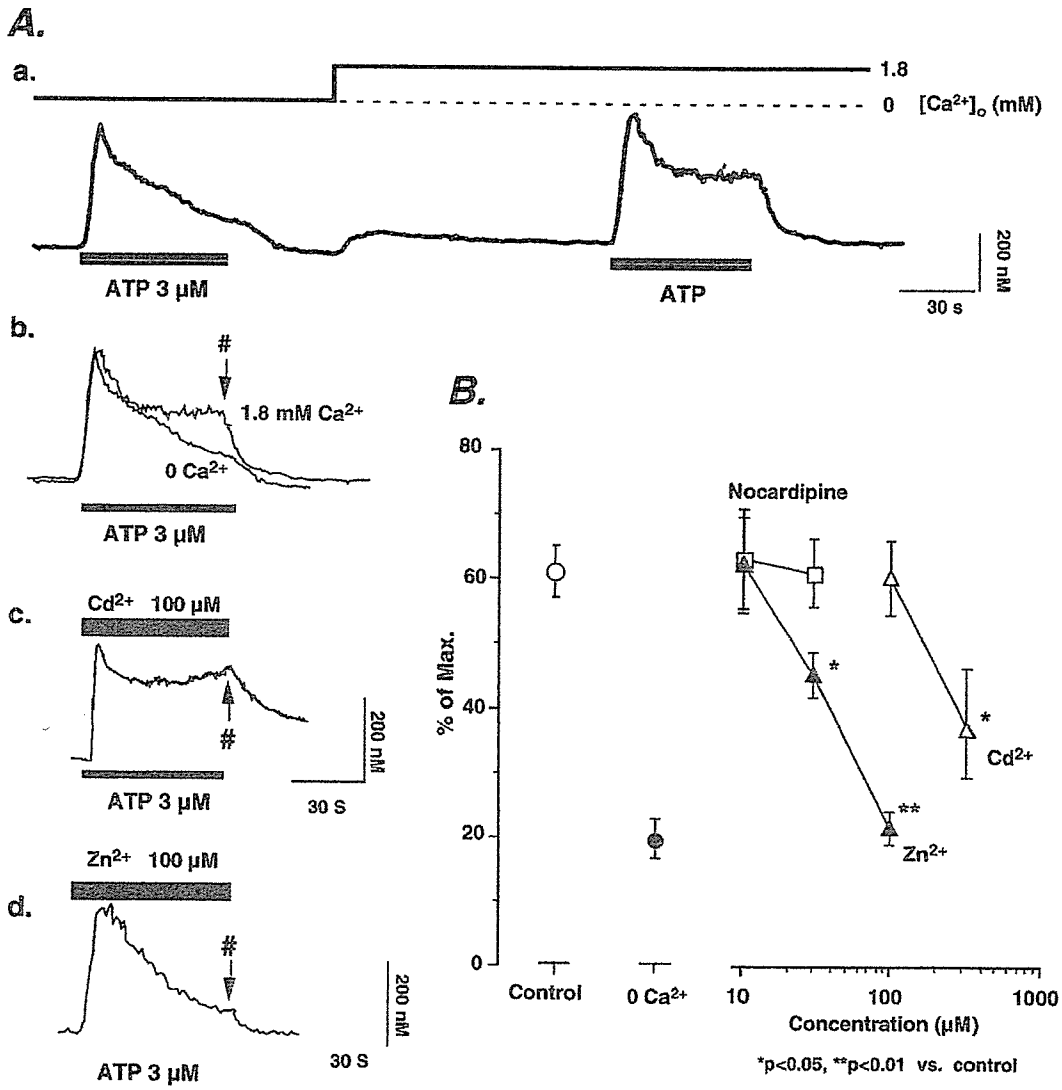

Fig. 5. Time-course of the elevation in $[Ca^{2+}]i$ evoked by ATP (1 min). A, Typical Ca^{2+} responses to 3 μM ATP for 1 min (solid bar). a, Ca^{2+} responses to ATP in the absence (open bar: Ca^{2+}-free) and presence (dotted bar: 1.8 mM Ca^{2+}) of external Ca^{2+}. ATP was applied to the cells twice for 1 min separated by 2 min, and the first and the second ATP applications were performed in the absence and presence of extracellular Ca^{2+}, respectively. b, Comparison of the time-course of the ATP-evoked rise in $[Ca^{2+}]i$ in the absence (0 Ca^{2+}) and presence of extracellular Ca^{2+} (1.8 mM Ca^{2+}). The traces obtained with Fig. 3A-a were superimposed; # with arrow shows the termination of the ATP-application. c and d, Typical Ca^{2+} responses to ATP in the presence of 300 μM Cd^{2+} (c) and 100 μM Zn2+ (d). Cd^{2+} and Zn^{2+} were presented throughout the ATP-application. B, Comparison of the time-course of the ATP-evoked rise in $[Ca^{2+}]i$. Values show % of the maximal response 1 min after ATP-application (at #). The data are mean ± s.e.m. obtained from 44 (ATP alone), 8 (Ca^{2+}-FREE), 16 (nicardipine), 22 (Cd^{2+}), and 26–35 (Zn^{2+}; 10–300 μM) cells tested. Asterisks show significant differences from the response evoked by ATP alone (**$p < 0.01$).

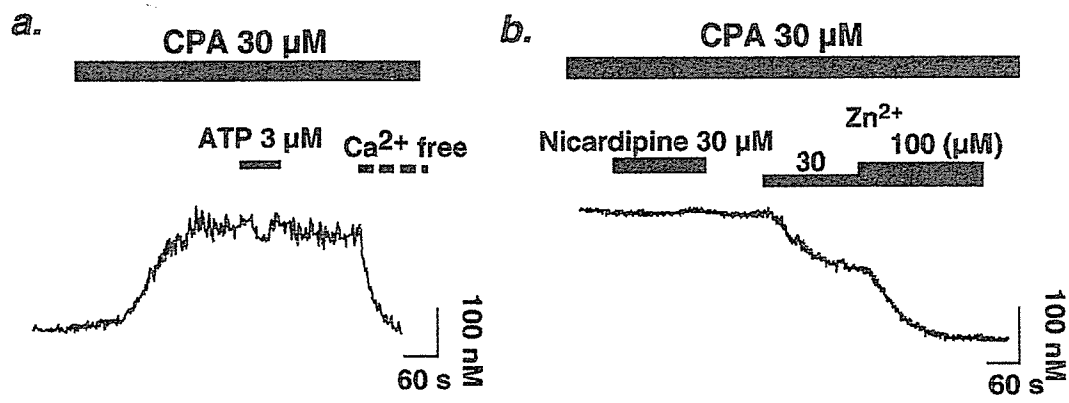

Fig. 6. Changes in $[Ca^{2+}]i$ in the hippocampal astrocytes evoked by CPA. a, The rise in $[Ca^{2+}]i$ evoked by 30 μM CPA (horizontal open bar). Five min after treatment with CPA, ATP (3 μM) was applied to the cells for 1 min (horizontal filled bar). The sustained $[Ca^{2+}]i$ was declined to the resting level by Ca^{2+}-free (n = 47 from 3 experiments). b, The effects of nicardipine (30 μM) and Zn^{2+} (30 and 100 μM) on the sustained rise in $[Ca^{2+}]i$ evoked by 30 μM CPA. Zn^{2+} but not nicardipine, inhibited the CPA-evoked Ca^{2+} responses (n = 41, 3 experiments). Vertical and horizontal scale bars show 100 nM and 60 s, respectively.

manner. Neither Cd^{2+} (100 μM) (Fig. 5A-c) nor nicardipine (30 μM) (Fig. 5B) affected the transient nor sustained responses, suggesting that voltage-gated Ca^{2+} channels do not contribute to these responses. On the other hand, Zn^{2+} significantly inhibited the sustained response (Fig. 5A-d and B), suggesting that this component is not mediated by channel forming P2X receptors [14], but by metabotropic P2Y receptors [13]. The sustained responses were significantly inhibited by Ca^{2+}-depletion or addition of Zn^{2+} (30 and 100 μM).

Changes in $[Ca^{2+}]i$ evoked by cyclopiazonic acid (CPA)

CPA (30 μM), an inhibitor of the Ca^{2+}ATPase pump of the endoplasmic reticulum, produced a sustained rise in $[Ca^{2+}]i$ only in the presence of extracellular Ca^{2+} (Fig. 6a). Thapsigargin (10 nM), another Ca^{2+}ATPase inhibitor, also produced a similar extracellular Ca^{2+}-dependent sustained $[Ca^{2+}]i$ elevation (data not shown). The CPA-evoked sustained $[Ca^{2+}]i$ elevation was inhibited by Zn^{2+} (30–100 μM) but not by 30 μM nicardipine (Fig. 6b). When the cells were pretreated with CPA (30 μM) for 5 min, additional application of ATP failed to evoke both the transient and the sustained rises in $[Ca^{2+}]i$ (Fig. 6a).

Discussion

We have characterized spatio-temporal Ca^{2+} signals evoked by ATP in cultured rat hippocampal astrocytes. ATP produced hierarchical Ca^{2+} signals, i.e., elementary Ca^{2+} release events, "puffs," global Ca^{2+} release, and CCE. These Ca^{2+} responses to ATP appear to be due to direct activation of P2 receptors because they were not inhibited by antagonists to various receptors including glutamate receptors, but was sensitive to suramin, an antagonist to P2 receptors.

ATP even at sub-threshold concentrations (<10 nM) evoked elementary Ca^{2+} release events in the majority of astrocytes. Such elementary Ca^{2+} signals were observed even in the absence of extracellular Ca^{2+}, suggesting that they were due to Ca^{2+} release from stores. The elementary Ca^{2+} signals were brief (lifetime ~ 1 second) and $[Ca^{2+}]_i$ increases had a spatial spread of approximately 3–6 μm. In control cells, the amplitudes of the elementary events typically ranged from 80–100 nM and the frequency was generally less than 0.1 Hz (0.06–0.1 Hz). All these characteristic features are well in accord with elementary Ca^{2+} events previously described in other cells [3,16]. Without stimulation, there were few puffs in the cells. However, upon stimulation with ATP, the number of cells showing elementary Ca^{2+} signals increased, as did the number of active elementary Ca^{2+} release sites within individual cells. In addition, the frequency of the events was dramatically enhanced (Fig. 1). Global Ca^{2+} signals arise via the coordinated recruitment of elementary Ca^{2+} release sites [3,16]. The switch from elementary to global Ca^{2+} signals in astrocytes can be achieved by increasing the stimulus concentration (Fig. 1). It is also reported that Ca^{2+} loading of the endoplasmic reticulum is an important factor for the switch in neuronal cells [16,15]. It would be interesting to clarify how astrocytic puffs could be switched into global Ca^{2+} signals in astrocytes.

The rise in $[Ca^{2+}]$i evoked by briefly applied ATP was not affected by removal of extracellular Ca^{2+}, suggesting involvement of metabotropic P2Y receptors in the Ca^{2+} responses [6]. In fact, ATP stimulated $InsP_3$ formation with an ED_{50} value similar to that of the Ca^{2+} response to ATP (Figs. 4, 6). The rank order of the responses was 2MeSATP > ADP = ATP > ATPγS > UTP. AMP and αβ-MeATP had no effect (Fig. 3). Except for UTP (agonist to P2Y2 receptors), this rank order well fits P2Y1 subclasses. Because of the diversity of cultured hippocampal astrocytes, multiple types of cells might be present in the preparations we used; i.e., some cells possess P2Y1 receptors and other cells may possess P2Y2 receptors. However, almost all astrocytes that responded to 2MeSATP also responded to UTP, which may exclude the above interpretation of different receptor populations among cells. Two functionally distinct P2 receptors are found to co-exist in rat phaeochromocytoma PC12 cells [13] and aortic endothelial cells [17]. Thus, it is probable that multiple types of P2 receptors, i.e., P2Y1 and P2Y2 receptors, exist in the same hippocampal astrocytes.

When ATP was applied to the cells for longer periods, it produced a transient $[Ca^{2+}]$i rise, followed by a sustained one (Fig. 5A-a). The sustained component seems to be mediated by Ca^{2+} influx from external spaces because this sustained response was abolished by external Ca^{2+}-depletion (Fig. 5A-a). Cd^{2+} or nicardipine had no effect on the Ca^{2+} influx, but Zn^{2+} significantly inhibited it, suggesting that the route of the Ca^{2+}influx is not voltage-gated Ca^{2+} channels but a Zn^{2+} sensitive Ca^{2+} permeable ionic pathway(s). A similar sustained Ca^{2+} entry has already been reported in PC12 cells [13], mast cells [8], and chick retina [19]. The ATP-evoked Ca^{2+} entry could be activated by a decrease of luminal Ca^{2+} concentration because (1) sustained Ca^{2+} entry was mimicked by CPA or thapsigargin, inhibitors of the Ca^{2+}ATPase pump of the endoplasmic reticulum (Fig. 6a), (2) pretreatment of cells with CPA abolished subsequent Ca^{2+} response to ATP, which indicates the overlap of Ca^{2+} entry mechanisms (Fig. 6a), and (3) both of the sustained $[Ca^{2+}]$i rises evoked by ATP and CPA were non-voltage dependent but were sensitive to Zn^{2+} (Figs. 5, 6b). These results strongly suggest that the hippocampal astrocytes possess CCE in response to depletion of Ca^{2+} stores and that the ATP-evoked sustained rise in $[Ca^{2+}]$i is dependent upon the filling states of $InsP_3$-sensitive Ca^{2+} stores.

Concentrations of synaptic Zn^{2+} that could be released [1] in the hippocampus have been estimated to be as high as 100–300 μM [5], which may be enough to inhibit the Ca^{2+} responses to ATP because regulation by Zn^{2+} occurred at concentrations under 100 μM (Fig. 6). ATP has also been reported to be

released by excitatory stimulation from hippocampal nerve endings [22,9]. In addition to neuronal cells, endogenous ATP seems to be able to act on glial cells to promote a rise in $[Ca^{2+}]i$ in the hippocampus, which could be regulated by released Zn^{2+}. Thus, it is suggested that both the ATP-evoked CCE and its inhibition by Zn^{2+} occur in the hippocampal astrocytes *in situ*, and that the regulation may be physiologically an event of great consequence.

In summary, we demonstrated here that ATP could produce the hierarchical organization of Ca^{2+} release from puffs to larger subcellular Ca^{2+} release, which subsequently leads to CCE. Astrocytes may use such hierarchical Ca^{2+} signals to process complex information. It should be emphasized that such hierarchical Ca^{2+} signals or CCE evoked by ATP and its inhibition by Zn^{2+}, could occur in the hippocampus *in situ*.

Acknowledgements

We appreciate Ms. T. Obama for culturing the cells, Dr. R. Teshima for helpful discussions, Dr. J. Kenimer for improving the manuscript, and Dr. Y. Ohno for continuous encouragement. This work was supported by the Human Science Foundation in Japan.

References

[1] Assaf SY, Chung SH. Release of endogenous Zn^{2+} from brain tissue during activity. Nature 1984;308:734–6.
[2] Berridge MJ. Capacitative calcium entry. Biochemical Journal 1995;312:1–11.
[3] Bootman MD, Berridge MJ, Lipp P. Cooking with calcium: the recipes for composing global signals from elementary events. Cell 1997;91:367–73.
[4] Emptage NJ, Reid CA, Fine A. Calcium stores in hippocampal synaptic boutons mediate short-term plasticity, store-operated Ca^{2+} entry, and spontaneous transmitter release. Neuron 2001;29:197–208.
[5] Frederickson CJ, Moncrieff DW. Zinc-containing neurons. Biology and Signals 1994;3:127–39.
[6] Fredholm BB, Abbracchio MP, Burnstock G, Daly JW, Harden TK, Jacobson KA, Leff P, Williams M. Nomenclature and classification of purinoceptors. Pharmacological Review 1994;46:143–56.
[7] Guthrie PB, Knappenberger J, Segal M, Bennett MV, Charles AC, Kater SB. ATP released from astrocytes mediates glial calcium waves. Journal of Neuroscience 1999;19:520–8.
[8] Hoth M, Penner R. Depletion of intracellular calcium stores activates a calcium current in mast cells. Nature 1992; 355:353–6.
[9] Inoue K, Koizumi S, Nakazawa K. Glutamate-evoked release of adenosine 5′-triphosphate causing an increase in intracellular calcium in hippocampal neurons. Neuroreport 1995;6:437–40.
[10] Kastritsis CH, Salm AK, McCarthy K. Stimulation of the P2Y purinergic receptor on type 1 astroglia results in inositol phosphate formation and calcium mobilization. Journal of Neurochemistry 1992;58:1277–84.
[11] Kimball BC, Mulholland MW. Enteric glia exhibit P2U receptors that increase cytosolic calcium by a phospholipase C-dependent mechanism. Journal of Neurochemistry 1996;66:604–12.
[12] Kirischuk S, Moller T, Voitenko N, Kettenmann H, Verkhratsky A. ATP-induced cytoplasmic calcium mobilization in Bergmann glial cells. Journal of Neuroscience 1995;15:7861–71.
[13] Koizumi S, Nakazawa K, Inoue K. Inhibition by Zn^{2+} of uridine 5′-triphosphate-induced Ca^{2+}-influx but not Ca^{2+}-mobilization in rat phaeochromocytoma cells. British Journal of Pharmacology 1995;115:1502–8.
[14] Koizumi S, Ikeda M, Inoue K, Nakazawa K. Enhancement by zinc of ATP-evoked dopamine release from rat pheochromocytoma PC12 cells. Brain Research 1995;673:75–82.
[15] Koizumi S, Lipp P, Berridge MJ, Bootman MD. Regulation of ryanodine receptor opening by lumenal Ca^{2+} underlies quantal Ca^{2+} release in PC12 cells. Journal of Biological Chemistry 1999;274:33327–33.

[16] Koizumi S, Bootman MD, Bobanovic LK, Schell MJ, Berridge MJ, Lipp P. Characterization of elementary Ca^{2+} release signals in NGF- differentiated PC12 cells and hippocampal neurons. Neuron 1999;22:125–37.
[17] Motte S, Pirotton S, Boeynaems JM. Heterogeneity of ATP receptors in aortic endothelial cells. Involvement of P2Y and P2U receptors in inositol phosphate response. Circulation Research 1993;72:504–10.
[18] Putney Jr JW. A model for receptor-regulated calcium entry. Cell Calcium 1986;7:1–12.
[19] Sakaki Y, Sugioka M, Fukuda Y, Yamashita M. Capacitative Ca^{2+} influx in the neural retina of chick embryo. Journal of Neurobiology 1997;32:62–8.
[20] Takeda M, Nelson DJ, Soliven B. Calcium signaling in cultured rat oligodendrocytes. Glia 1995;14:225–36.
[21] Verkhratsky A, Kettenmann H. Calcium signalling in glial cells. Trends in Neuroscience 1996;19:346–52.
[22] Wieraszko A, Goldsmith G, Seyfried TN. Stimulation-dependent release of adenosine triphosphate from hippocampal slices. Brain Research 1989;485:244–50.

ELSEVIER

Neuroscience Letters 318 (2002) 113–116

Neuroscience Letters

www.elsevier.com/locate/neulet

Inversion of the anatomical lateralization of chick thalamofugal visual pathway by light experience

Mamiko Koshiba[a,b], Tateki Kikuchi[c], Masafumi Yohda[b], Shun Nakamura[a,*]

[a]Division of Biochemistry and Cellular Biology, National Institute of Neuroscience, NCNP, Tokyo 187-8502, Japan
[b]Department of Biotechnology and Life Sciences, Tokyo University of Agriculture and Technology, Tokyo 184-8588, Japan
[c]Division of Animal Models for Human Disease, National Institute of Neuroscience, NCNP, Tokyo 187-8502, Japan

Received 3 September 2001; received in revised form 10 September 2001; accepted 17 September 2001

Abstract

It has been reported that light exposure to one eye induces functional lateralization, which can be inverted by exposing the opposite eye to the light. However, the anatomical basis of the functional inversion by the light has not been shown. To address this issue, we labeled cells in the dorsolateral anterior thalamus (DLA) using retrograde fluorescent tracers injected into visual Wulst, counted the labeled cell number, and compared the anatomical asymmetry of DLA between the left eye occluded and the right eye occluded chickens. We found that a rostral part of DLA (DLAda) and a lateral/ventral part of DLA differentially projected to the visual cortex ipsilaterally and contralaterally, respectively. These regions showed anatomical asymmetry that was inverted by the light. An antibody against a nicotinic acetylcholine receptor subunit more intensively and widely stained the side of DLA receiving the light stimulation and the cell labeled by the tracers co-localized with the immunoreactive neuropil. These results indicated that the light experience induced the anatomical lateralization of thalamofugal visual pathway. © 2002 Elsevier Science Ireland Ltd. All rights reserved.

Keywords: Lateralization; Light experience; Visual Wulst; Thalamofugal pathway; Nicotinic acetylcholine receptor; α-Bungarotoxin

Avian has two kinds of visual pathway, tectofugal pathway and thalamofugal pathway; visual tasks requiring higher information processing, but not simple brightness, color or pattern discriminations depend on the latter pathway, and the thalamofugal pathway, but not tectofugal pathway shows functional and anatomical lateralization [5]. The functional lateralization is regulated by light experience only for a few hours during embryonic days just before hatching [3]. We investigated the role of light experience to know whether this role is permissive or instructive. In order to study this point, we set up two experimental conditions, the left eye occluded (normal developmental condition) and the right eye occluded conditions during the critical period [3] for development of the thalamofugal pathway. Then, we asked whether anatomical asymmetry could be inverted or not under two experimental conditions.

First of all, we investigated the anatomical asymmetry in thalamofugal pathway using fluorescent retrograde tracers as described in Fig. 1. Embryos were incubated in the dark until the 19th day of incubation (E19). The eye patch was applied essentially as described by Rogers [4] at E20 and the embryos were further reared under the light illumination. On the 2nd day after hatching (P2), two fluorescent dyes were stereotaxically injected separately into each hemisphere under a surgical microscope (Nagashima Co. Ltd., Tokyo, Japan) [2]. After incision of the scalp, the injection point on the skull was defined at 5 mm anterior from the intersection point of the midline and the boundary between cortex and cerebellum, 1 mm lateral from the midline and 1.7 mm deep from the skull. Chicken was killed at P6 and frozen sections (50 μm thickness) were prepared [8]. We analyzed only male chicken to avoid any complexity between sexes [7]. The tracer injection sites at P6 were located at 2.6 ± 0.7 mm (mean ± SD, $n = 14$) from the anterior edge of the brain, 1.1 ± 0.1 mm (mean ± SD, $n = 14$) lateral from the midline of the brain and 1.4 ± 0.2 mm (mean ± SD, $n = 14$) deep from the cortical surface, which occupied the hyperstriatum accessorium (HA) dorsal to lamina frontalis suprema (LFSM) (Fig. 1a, arrow). Images of the left and right thalamic nuclei were separately captured as a digitized image using a confocal microscopy (Amersham Pharmacia Biotech, Buckinghamshier, England). Then, an equivalent image was matched and presented as a pair image of the left and

* Corresponding author. Tel.: +81-423-46-1722; fax: +81-423-46-1752.
E-mail address: nakamura@ncnp.go.jp (S. Nakamura).

PII: S0304-3940(01)02306-0

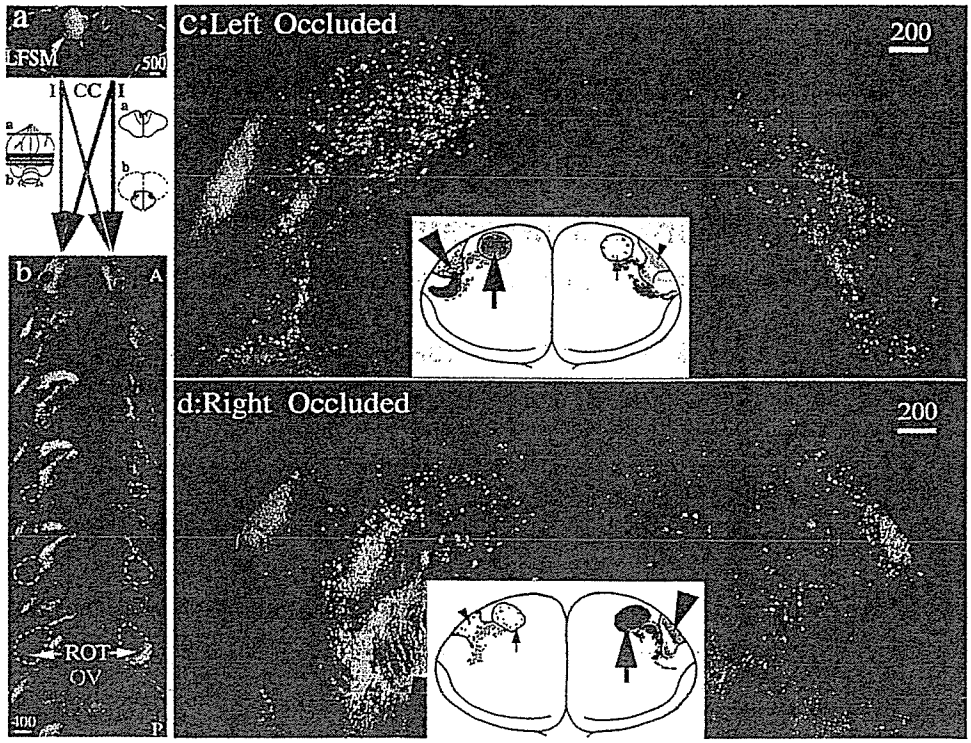

Fig. 1. Double staining pattern of thalamic nuclei using fluorescent retrograde tracers injected into each hemispheric hyperstriatum (HA). (a) Confirmation of the location of injection sites. A coronal section including the injection sites was presented. The tracer injected into the left and right hemispheric HA was 4Di10ASP (yellow-green) and DiI (red), respectively. (b) Serial presentation of thalamic nuclei stained by the fluorescent tracers. Coronal sections were serially prepared, and each one from three serial sections was aligned along anterior (A)–posterior (P) axis from the top to the bottom of the figure. (c,d) Anatomical asymmetry of thalamic nuclei revealed by the fluorescent tracers. Scale bars, 500 μm in (a); 400 μm in (b); 200 μm in (c,d).

right hemispheric thalamic nuclei based on comparing the shape of labeled cells as well as the size of nucleus rotundus (circled by white dotted line, ROT) and nucleus ovoidalis (circled by pink dotted line, OV). A serial presentation of thalamic nuclei (Fig. 1b) clearly showed that the ipsilaterally and contralaterally labeled cells appeared in both side of nucleus dorsolateralis anterior thalami (DLA) located rostral to nucleus rotundus (ROT) (see also Fig. 4a for the definition of DLA). In the DLA, we found the region where projections sent almost entirely to the ipsilateral HA and defined this region as DLA pars dosolateralis pars anterioris (DLAda) (arrows in Fig. 1c,d). The contralaterally labeled cells located separately and more laterally from DLAda (arrow heads in Fig. 1c,d). The asymmetry was found in these regions. In the case of the left eye occluded (Fig. 1c), DLAda was more heavily stained in the left side by the ipsilaterally injected dye (heavy arrow, yellow-green). The contralaterally labeled cells were more abundant also in the left side (heavy arrowhead, see below regarding quantitative analysis). In contrast, the right side appeared dominant in the case of the right eye occluded (Fig. 1d).

In order to obtain quantitative data, we calculated the relative ratio of the cell number in DLAda to the total ipsilaterally labeled cell number in DLA (DLAda ratio) to cancel variations of the labeled cell number among chickens (Fig. 2). The total labeled cell number varied among the

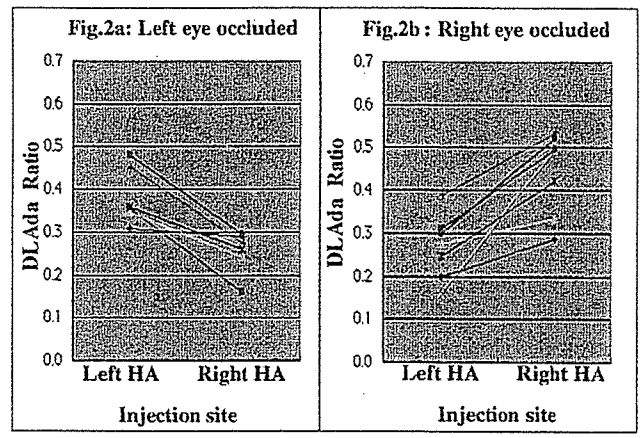

Fig. 2. The relative contribution of the labeled cell number in DLAda to the total ipsilaterally labeled cell number in DLA with the same tracer. The cell number was counted with slices after taking the confocal images using Mac SCOPE (Mitani Corporation, Fukui). Each one from three serial sections was used for this counting. The ratio (DLAda ratio) was compared between the brain samples prepared from the left eye occluded (a) and the right eye occluded (b) chickens ($n = 7$ in each case). The significance of the ratio between tracers was analyzed using the Wilcoxon two samples test. The value was considered as significant in the case of $P < 0.05$.

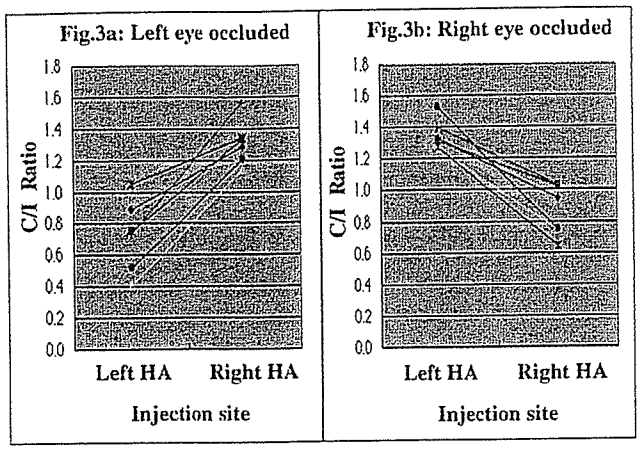

Fig. 3. Comparison of the C/I ratio between the left eye occluded and the right eye occluded condition. The C/I ratios of the left eye occluded (a) and the right eye occluded samples (b) ($n = 7$ in each case) were presented. The significance of the difference of the C/I ration between two tracers was analyzed using the Wilcoxon two samples test. The value was considered as significant in the case of $P < 0.05$.

chickens presumably because of variation of the amount of the injected dyes, ranging from 296 to 1440 cells (4DiASP) and from 260 to 889 cells (DiI) in the case of the left eye occluded chickens, and from 364 to 808 (4Di10ASP) and from 528 to 1367 (DiI) in the right eye occluded chickens, respectively. The DLAda ratio in the left thalamic nuclei was higher than that in the right side in the case of the left eye occluded. While, in the case of the right eye occluded, the ratio was significantly inverted (Fig. 2b). We next counted the contralaterally labeled cell number in DLA and calculated the ratio of this number to the ipsilaterally labeled cell number with the same tracer (C/I ratio). The contralaterally labeled cell number also varied from 265 to 1019 (4Di10ASP) and from 335 to 1167 (DiI) in the left eye occluded chickens, and from 511 to 1032 (4Di10ASP) and from 484 to 886 (DiI) in the right eye occluded chickens, respectively. Then, the C/I ratio for each tracer dye was compared. As shown in Fig. 3a, the C/I ratio was higher for the tracer (DiI) injected in the right HA than that (4Di10ASP) injected in the left HA in the case of the left eye occluded. Thus, we could confirm the observation reported by the Rogers group [6]. Importantly, the C/I ratio was inverted in the case of the right eye occluded (Fig. 3b). This is the first report that the anatomical inversion of thalamofugal pathway can be triggered by the light experience, indicating that the light experience has an instructive role on the development of anatomical lateralization of thalamofugal pathway.

We further asked the existence of any neurochemical marker in the cells labeled by the tracers. We tried a couple of antibodies including anti-thyrosine hydroxylase, choline acetyl transferase, γ-aminobutyric acid, and glutamic acid decarboxylase, etc. Among them, an antibody against nicotinic acetylcholine receptor (nAChR) subunit α8 stained the anterior part of thalamus as shown in Fig. 4, which corresponds to DLA as described by Britto [1]. At higher magnification (×66, data not shown), we observed the fuzzy staining structure suggesting neuropil, but not somata was mainly stained. Surprisingly, the anti-α8 more heavily and widely stained the left side of DLA that had received the light stimulation through the right eye (Fig. 4a, normal developmental condition). It should be noted that DLAda was more intensively stained in the left side, consisting with the observation of the higher relative tracer-labeled cell number in the left DLAda in the left eye occluded condition. This observation was reproducible in at least three indepen-

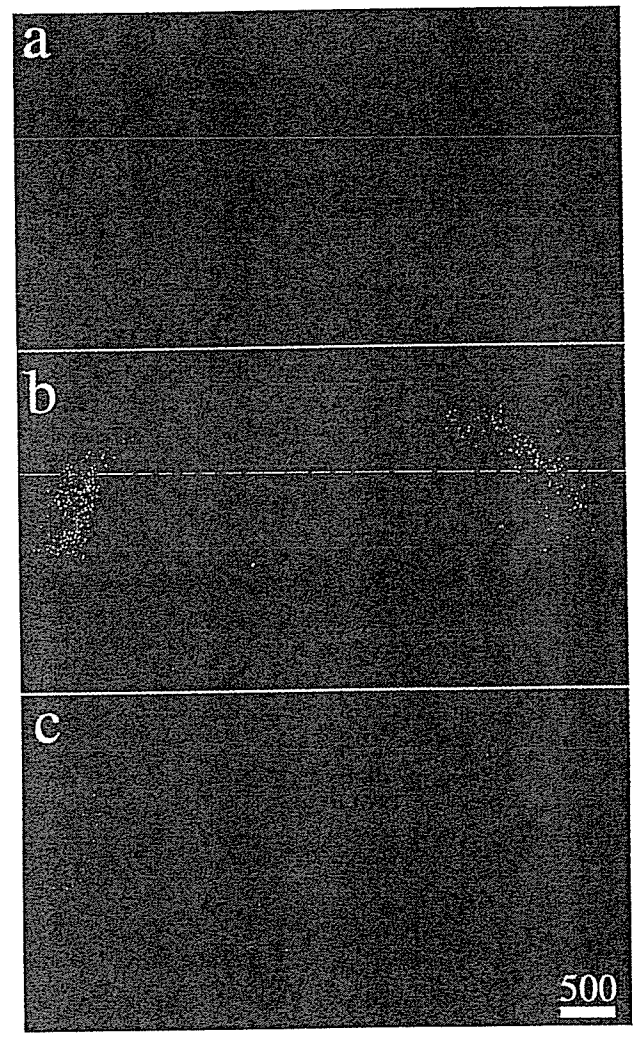

Fig. 4. Localization of the thalamic nuclei labeled by the retrograde tracers in DLA expressing nicotinic acetylcholine receptor (nAChR). (a) Immunostaining DLA with a monoclonal antibody to nAChR subunit α8 (Covance, Richmond, CA). Fluorescent (Cy3) imaging was captured and digitized by a CCD camera system equipped to a fluorescent microscope (Axiophoto2; Carl Zeiss Co. Ltd., Oberkochen). The chickens were reared under normal light illumination condition without eye-patch. (b) Localization of cell bodies labeled by a tracer in DLA. Fluorogold (FG) was injected into the right side of HA essentially as described in the text. (c) An overlaid image of FG and nAChR staining using Photoshop. Scale bar, 500 μm.

dent experiments. Fluorogold (FG) was used for a retrograde tracer at the same time and injected only in the right HA (Fig. 4b). We found FG-labeled cells co-localized in the region stained by the anti-α8 (Fig. 4c). In the α8-positive region, the ipsilaterally labeled cells (the right side) occupied the dorsal part of DLA (DLAda) and the contralaterally labeled cells (the left side) occupied the lateral/ventral part of DLA. This result suggests that the thalamofugal projection neurons in DLA may receive cholinergic regulation.

Taken together, these results suggest that the light experience plays an instructive role on the lateralization of thalamofugal pathway in such a way that more prominent projections develop in the hemisphere receiving light stimulation during the critical period.

This research was supported by a grant of advanced brain research from the ministry of Education, Science, Sports, Culture, and Technology of Japan and by health sciences research grants on human genome, tissue engineering, and food biotechnology from the Ministry of Labor, Health and Welfare of Japan. We thank Director Giichi Nakamura (Mitaka Kohki Co. Ltd.) for providing a surgical microscope and Akemi Takayama for technical assistance.

[1] Britto, L.R., Keyser, K.T., Lindstrom, J.M. and Karten, H.J., Immunohistochemical localization of nicotinic acetylcholine receptor subunits in the mesencephalon and diencephalon of the chick (Gallus gallus), J. Comp. Neurol., 317 (1992) 325–340.
[2] Kuenzel, W.J. and Masson, M., A Stereotxic Atlas of the Brain of the Chick, The Johns Hopkins University Press, Baltimore, MD, 1988, pp. 1–13.
[3] Rogers, L.J., Light experience and asymmetry of brain function in chickens, Nature, 297 (1982) 223–225.
[4] Rogers, L.J., Light input and the reversal of functional lateralization in the chicken brain, Behav. Brain Res., 38 (1990) 211–221.
[5] Rogers, L.J. and Deng, C., Light experience and lateralization of the two visual pathways in the chick, Behav. Brain Res., 98 (1999) 277–287.
[6] Rogers, L.J. and Bolden, S.W., Light-dependent development and asymmetry of visual projections, Neurosci. Lett., 121 (1991) 63–67.
[7] Schwarz, I.M. and Rogers, L.J., Testosterone: a role in the development of brain asymmetry in the chick, Neurosci. Lett., 146 (1992) 167–170.
[8] Singh, T.D., Mizuno, K., Kohno, T. and Nakamura, S., BDNF and trkB mRNA expression in neurons of the neonatal mouse barrel field cortex: normal development and plasticity after cauterizing facial vibrissae, Neurochem. Res., 22 (1997) 791–797.